Bioresource Technology 220 (2016) 305–311

Contents lists available at ScienceDirect

Bioresource Technology

journal homepage: www.elsevier.com/locate/biortech

Hydrothermal carbonization of tobacco stalk for fuel application

Jiaxiao Cai [a], Bin Li [a], Chaoying Chen [b], Jing Wang [a], Min Zhao [a], Ke Zhang [a,*]

[a] Zhengzhou Tobacco Research Institute of CNTC, Zhengzhou 450001, China
[b] Shanghai New Tobacco Institution, Shanghai 200082, China

HIGHLIGHTS

- Energy densified hydrochars were prepared by HTC of tobacco stalks.
- The effects of HTC temperature and time on fuel properties of hydrochars were investigated.
- Hydrochars were characterized by SEM, BET, EA, FTIR and TGA.
- The combustion performance of the hydrochars was improved compared to the starting TSs.

ARTICLE INFO

Article history:
Received 11 August 2016
Received in revised form 24 August 2016
Accepted 25 August 2016
Available online 27 August 2016

Keywords:
Tobacco stalk
Biomass
Hydrothermal carbonization
Hydrochar
Combustion

ABSTRACT

Tobacco stalks are an abundant biomass resource which are otherwise treated as waste. In this work, the effect of hydrothermal carbonization temperature and time on the structures, chemical compositions and combustion characteristics of hydrochars obtained from tobacco stalks were evaluated. The carbon content, higher heating value, and energy yield increased with accompanying decrease in hydrogen and oxygen contents with the increase of treatment temperature and time. The evolution of the H/C and O/C atomic ratios indicated dehydration and devolatilization processes occurred during hydrothermal carbonization. The weight loss, combustion range and characteristic temperatures of tobacco stalks were significantly modified after hydrothermal carbonization, resulting in higher ignition temperatures and higher energy density. The kinetics model, Coats–Redfern method revealed the activation energy of hydrochars in zone 2 and 3 were among 43.7–74.8 kJ/mol and 46.7–85.8 kJ/mol, respectively. Our results show that hydrothermal carbonization reaction can facilitate transforming tobacco stalks into energy-rich solid fuel.

1. Introduction

Tobacco stalks (TSs) are the biomass waste after tobacco harvesting. The yield of TSs in tobacco production is around 20% (Yang et al., 2012), far more than any other tobacco waste (tobacco stems, tobacco debris, et al.). Therefore, great economic benefits can be achieved by appropriate utilization of the waste TSs. Conventional methods for disposing TSs include burning or discarding them in the farmland, not only bringing about serious environmental pollution issues but also resulting in the wastage of renewable biomass resources.

To date, the literature published on biomass utilization with respect to the disposal of tobacco waste via novel approaches including: (1) preparation of activated carbons with specific surface area and nitrogen/heteroatom content by calcination, hydrothermal carbonization (HTC) or microwave radiation methods (Kilic et al., 2011; Li et al., 2008; Sha et al., 2015; Zhao et al., 2016); (2) extracting nicotine and solanesol through the column-chromatographic extraction (Hu et al., 2015). However, these methods are problematic for large-scale industrial production since they need long processing time and multifarious procedures with high costs. An alternative cost-effective way to address this problem is to employ the tobacco waste as biofuels for combustion to liberate energy like other types of lignocellulosic biomass (Lai et al., 2012; Li et al., 2011; Ragauskas et al., 2006). However, raw tobacco waste possesses certain inherent drawbacks such as low heating value, high moisture, high oxygen contents, and high alkaline earth metal content, making it unsuitable for being burned directly on a large scale. Accordingly, converting this tobacco waste into a higher energy density form before combustion is of great importance.

Pyrolysis is the most commonly utilized process for biomass conversion which occurs in the absence of oxygen to obtain high

* Corresponding author.
E-mail address: hfzhangke@126.com (K. Zhang).

http://dx.doi.org/10.1016/j.biortech.2016.08.098
0960-8524/

Nomenclature

α	conversion fraction	A	pre-exponential factor
t	time	E_a	activation energy of the reaction
k	reaction rate constant	T	thermodynamic temperature
$f(\alpha)$	general expression of the reaction mechanism	β	constant heating rate
m_i	initial sample mass	$G(\alpha)$	integral function of conversion
m	current sample mass	R^2	correlation coefficient
m_f	final sample mass		
n	order of reaction		

heating value products like lignite-type coal called biochar (White et al., 2011). Nevertheless, tobacco waste need to be dried before pyrolysis and the pyrolysis temperature is relatively high, which results in the increase of energy consumption. Besides, large amount of noxious gases were produced during pyrolysis, it requires a set of tail gas treating plant (Bassilakis et al., 2001). In this context, hydrothermal carbonization would be a better choice to overcome these drawbacks of pyrolysis mentioned above.

HTC, a facile and eco-friendly process used to prepare a solid coal-like product called hydrochar at moderate temperature under autogenous pressure, shows more significant advantages than pyrolysis. The process avoids an energy-extensive drying process, relatively low operation temperature, fewer gaseous products, and high conversion efficiency (Huff et al., 2014; Zhao et al., 2014). Hydrochar is obtained from a series of hydrolysis, condensation, dehydration and decarboxylation reactions in the HTC process of biomass (Titirici et al., 2008). Similar to the biochar produced from pyrolysis, the hydrochar also possesses higher fuel properties than raw biomass, such as higher carbon content, lower oxygen content, higher heating value, higher energy density and lower emission of greenhouse gases (Islam et al., 2015; Kang et al., 2012).

To the best of our knowledge, no systematic studies have ever been done focusing on the solid fuel production prepared by HTC of TSs. Herein, this study expanded the utilization of tobacco waste, namely TSs, by converting them from waste into solid biofuel via HTC. The main objectives of this study were to investigate the effects of HTC reaction temperature and reaction time on the chemical, structural and combustion characteristics of hydrochar, thus to evaluate the potential fuel properties of TSs before and after HTC process.

2. Material and methods

2.1. Materials

TSs were obtained from Xiangxian, Henan Province in China. The samples were cut into small pieces and washed with tap water followed by distilled water to remove any dirt or dust. After that, the chips of TSs were dried naturally under the sun for 3 days and then crushed into fine particles with the diameter under 1 mm using a grinder and subsequently stored in a sealed container until use.

2.2. Hydrothermal carbonization process

The HTC process of TSs was conducted in a 30 mL Teflon-lined autoclave. In a typical synthesis, 2 g of prepared TSs powder was homogenously mixed with 20 mL deionized water and then transferred into the autoclave and sealed. The experimental conditions of HTC were divided into two parts: heating at different temperatures (180 °C, 200 °C, 220 °C, 240 °C, 260 °C) with a constant reaction time of 2 h and holding at different reaction time (1 h, 2 h, 4 h, 8 h, 12 h) with a constant temperature of 260 °C. The autoclave was sealed and loaded in an electric furnace, heated to the desired reaction temperature with a heating rate of 5 K/min. Subsequently, the autoclave was quickly immersed into cold water to cease the reaction after the specified residence time. The resulting coal-like solid product (hydrochar) was recovered by vacuum filtration and washed with distilled water, followed by drying to a constant weight in an oven at 105 °C for 9 h. The TSs derived hydrochars were denoted as reaction temperature-residence time, e.g. the sample prepared at 180 °C with reaction time of 2 h was labeled as 180-2. The yield of hydrochar was calculated by the following equations:

$$\text{Yield}\ \ (\%) = \frac{\text{Hydrochar weight}}{\text{TSs feedstock weight}} \times 100\%$$

2.3. Characterization

The proximate analyses of TSs and the derived hydrochars were performed in accordance with standards prescribed by the American Society for Testing and Materials (ASTM) to determine the weight percentages of moisture content (M), volatile components (VM) and fixed carbon (FC) and ash. The C, H, N, S and O elemental analysis was carried out in an elemental analyser (Vario EI Cube, Elementar, Germany) with a mass of about 3 mg. Furthermore, the proximate and elemental analysis of each sample were performed three times in the corresponding instruments and then took an average. Fourier Transform Infrared (FTIR) spectroscopy measurements was conducted by a Nicolet 6700 FTIR spectrometer (Themo Scientific, US) with the KBr pellet technique. It was recorded in the 4000–400 cm^{-1} region with 124 scans per sample.

The surface morphology of the TSs and hydrochars was characterized by scanning electron microscopy (SEM JEOL-6010LA, Japan). Before imaging, samples were placed onto adhesive carbon tape and sputtered with gold using a Sputter Coater (JEOL JFC-1600, Japan). The accelerating voltage and the working distance were 10 kV and 10 mm, respectively. Nitrogen adsorption and desorption isotherms were then taken at 77 K using a surface area analyzer (Tristar II 3020, US). According to the resulting N_2 adsorption–desorption isotherms of the samples, the Brunauer–Emmett–Teller (BET) method and Barrett-Johner-Halendar (BJH) method were used to analyze the specific surface areas (S_{BET}) and total pore volume (V_t) in the mesoporous range, respectively.

Thermal gravimetric analysis (TGA) was performed in simulated air (V_{N2} = 80%, V_{O2} = 20%) and at flow rate 30 mL/min with a heating rate of 10 K/min from 30 to 800 °C to measure combustion characteristics of the samples (approximate 10 mg was used) by using a thermogravimetric analyzer (STA 449F3, NETZSCH, Germany). The TG and DTG (the first derivative of TG curve) profiles were analyzed to derive key combustion parameters such as ignition temperatures, peak temperatures and burnout temperatures in accordance with the literatures published previously (Liu and

Balasubramanian, 2012; Parshetti et al., 2013). The ignition temperature (T_0) was the temperature the fuel begins to burn, determined by the beginning temperature of the devolatilization, the temperature with the maximum DTG value and the corresponding slope to the intersection with respect to the TG curve. The peak temperatures were obtained corresponding to the peak values of the DTG profiles. The burnout temperature (T_f) was detected when the weight loss was constant.

2.4. Determination of the kinetic parameters

The combustion process of solid materials is assumed to be composed of simple thermochemical reactions and the combustion kinetics was calculated by the decomposition rate of samples described as follows (Gil et al., 2010; Islam et al., 2016; Zhao et al., 2014):

$$\frac{d\alpha}{dt} = kf(\alpha) \tag{1}$$

$$\alpha = (m_i - m)/(m_i - m_f) \tag{2}$$

$$f(\alpha) = (1-\alpha)^n \tag{3}$$

where α is the conversion fraction obtained from TG-DTG data, and $d\alpha/dt$ refers to the rate of conversion at time t; $f(\alpha)$ represents the general expression of the reaction mechanism; m_i, m and m_f denote the initial, current and final sample mass of the sample, respectively; n is the order of reaction; and k is the reaction rate constant given by the Arrhenius equation:

$$\mathrm{k} = A\exp\left(-\frac{E_a}{RT}\right) \tag{4}$$

where A is the pre-exponential factor, E_a is the activation energy of the reaction, and T is the thermodynamic temperature.

Combined Eqs. (1), (3) and (4) can obtain:

$$\frac{d\alpha}{dt} = A\exp\left(-\frac{E_a}{RT}\right)(1-\alpha)^n \tag{5}$$

For a constant heating rate β (K/min) during combustion, $\beta = \frac{dT}{dt} = \frac{dT}{d\alpha} \times \frac{d\alpha}{dt}$, Eq. (5) can be transformed into:

$$\frac{d\alpha}{dT} = \frac{A}{\beta}\exp\left(-\frac{E_a}{RT}\right)(1-\alpha)^n \tag{6}$$

Integrating Eq. (6) becomes:

$$G(\alpha) = \int_0^x \frac{d\alpha}{(1-\alpha)^n} = \frac{A}{\beta}\int_{T_0}^{T}\exp\left(-\frac{E_a}{RT}\right)dT \tag{7}$$

where $G(\alpha)$ is the integral function of conversion.

In this work, the kinetic parameters of non-isothermal combustion process were derived using Coats-Redfern approximation method (Coats and Redfern, 1964). Therefore, based on Coats-Redfern method Eq. (7) is transformed into the following logarithmic form:

$$\ln\left[\frac{G(\alpha)}{T^2}\right] = \ln\left[\frac{AR}{\beta E}\left(1-\frac{2RT}{E}\right)\right] - \frac{E}{RT} \tag{8}$$

For easy calculation, Eq. (8) can be described as:

$$\ln\left[\frac{G(\alpha)}{T^2}\right] = \ln\left(\frac{AR}{\beta E}\right) - \frac{E}{RT} \tag{9}$$

A plot of $\ln[G(\alpha)/T^2]$ against $-1/T$ gives a straight line. Hence, E_a and A can be calculated from the slope and the intercept. The theoretical expressions of $G(\alpha)$ for the three kinetic model mechanisms were employed for the kinetic study of the combustion process of solid materials (Table S1). Besides, the form of $G(\alpha)$ which results in a straight line with the highest correlation coefficient (R^2) will be considered the expression of the model which best represents the kinetics of mass loss for each separate reaction.

3. Results and discussion

3.1. Structural properties of the hydrochar

Compared with raw TSs (lemon yellow), the color of hydrochar samples became darker with the increase of hydrothermal carbonization temperature and reaction time which consistent with partially carbonized biomass. SEM images were used to investigate the apparent morphology changes of hydrochar derived from different reaction temperatures (Fig. S1, see Supplementary Information) and times (Fig. S2, see Supplementary Information). The SEM image of the raw TSs shows a relatively glossy and well-defined surface, typical of lignocellulosic structure, whereas the degree of surface roughness increased gradually as the reaction temperature increased from 180 °C to 220 °C. This could be ascribed to the decomposition of hemicellulose as well as the depolymerisation of cellulose and partially degradation of lignin (Kambo and Dutta, 2015; Sevilla and Fuertes, 2009b). When the reaction temperature increased to 260 °C, the original structure was almost destroyed and broken into pieces, indicating that a higher reaction temperature accelerated the degradation of lignocellulosic structure (Funke and Ziegler, 2010). The surface morphology of the sample 260-1 was much rougher than the starting TSs and similar to the 200-2, while it could be hardly seen any lignocellulosic structure in 260-4, 260-8 and 260-12 because of the ruptured and extremely irregular porous surface. Interestingly, there were numerous sphere-like microparticles produced on the surface of the 260-8 and 260-12 hydrochars. The possible reason for the microparticles formation was attributed to the much higher reaction temperature (260 °C) and longer reaction time (8 h and 12 h) in the HTC process. Because high temperature with a long reaction time may facilitate the dehydration, condensation, or polymerization and aromatization reactions of the cellulosic components which give rise to the formation of ball-shaped microparticles (Sevilla and Fuertes, 2009a).

The porous textural characteristics were assessed by nitrogen physisorption method. These samples were found to exhibit small BET surface areas and a poor porosity (Table 1). The BET surface of the raw TSs was only 1.029 m^2/g and the total pore volume was 0.002 cm^3/g, respectively. These values gradually increased with the increase of hydrothermal temperature and time, while the highest BET surface areas and total pore volume of the hydrochar samples shown in Table 1 were relatively low (11.272 m^2/g and 0.057 cm^3/g, respectively) and close to the poor porosity of hydrochars previously reported (Parshetti et al., 2013; Reza et al., 2015; Sevilla and Fuertes, 2009a). Noticeably, the BET surface and total pore volume began to decrease when increasing reaction time

Table 1
Textural parameters calculated from the N_2 adsorption of TSs and hydrochars obtained from HTC of raw TSs.

Sample	S_{BET} (m^2/g)	V_t (cm^3/g)	Average pore diameter (nm)
TS	1.029	0.002	6.016
180-2	1.294	0.004	7.070
200-2	2.403	0.008	8.951
220-2	2.649	0.011	9.497
240-2	3.687	0.016	10.841
260-2	7.253	0.030	12.590
260-1	2.661	0.011	9.251
260-4	11.272	0.057	14.866
260-8	7.164	0.030	10.387
260-12	2.523	0.007	7.117

(temperature of 260 °C) to higher than 4 h, which may be ascribed to the formation of numerous sphere-like microparticles causing the destruction of porous channels. Moreover, the N_2 sorption isotherms of these all samples showed a type II isotherm (Fig. S3, see Supplementary Information), typical of non-porous or macroporous solids which have no framework-confined pores, and their surface area arises mainly from interparticle voids (Sevilla et al., 2011b).

3.2. Chemical characterization

The results of elemental composition analysis and hydrochar yield of the raw TSs and the derived hydrochars are summarized in Table 2. A higher recovery of solid product was obtained at lower temperatures, with nearly 80% of the feedstock mass recovery for sample 180-2. Nevertheless, a distinct decrease in the hydrochar yield could be seen with the increase of HTC temperature and time, which was possibly caused by the greater primary decomposition of the biomass structures or secondary decomposition of the solid residue, as reported previously (Parshetti et al., 2013; Zhao et al., 2014). The elemental composition of hydrochars obtained under different conditions changed noticeably as a result of carbonization. The carbon content increased from 46.2% to 65.2% along with a reduction in the hydrogen and oxygen contents, and the changing trend of elemental contents of TSs derived hydrochars were basically consistent with the HTC of grindelia and rabbitbrush reported previously (Reza et al., 2016). These changes could be clearly analyzed with the aid of a Van Krevelen diagram (Fig. 1) (Van, 1950). The Van Krevelen diagram clearly denotes that the evolution of the H/C-O/C atomic ratios from raw TSs to hydrochar samples followed essentially the paths of dehydration and decarboxylation, while the demethanation pathway was negligible, which was similar to the HTC of sewage sludge, cellulose and other kinds of lignocellulosic biomass (Dudder et al., 2016; He et al., 2013; Sevilla et al., 2011a,b). In this process possibly anhydride, ether, and lactone bonds were formed (Sevilla and Fuertes, 2009a). Besides, the dehydration and decarboxylation trends became increasingly apparent at higher operating temperatures and longer reaction time, and it came to be stable at operating temperature of 260 °C with reaction time longer than 8 h, indicating that the conversion of TSs during HTC process may be nearly complete at such long reaction time.

Table 3 shows the proximate analysis, higher heating value (HHV) and energy yield of TSs and hydrochars. The volatile matter of the raw TSs was 75.1%, but it gradually reduced after HTC reaction. Instead, the fixed carbon of hydrochar samples was much higher than that of the TSs feedstocks (15.2%). Both the volatile matters and fixed carbon changed significantly at higher operating temperature as well as longer holding time. For instance, the volatile components of sample 260-2 and 260-12 decreased to 64.9% and 42.4%, while the fixed carbon, increased to 26.8% and 48.8%, respectively. This illustrates further decomposition and carbonization of the lignocellulosic structure during HTC process at such high temperature with such long time (Parshetti et al., 2013), consistent with the results discussed in part 3.1. The HHV calculated by the formula developed by Song et al. (2012), raising up with the increase of HTC temperature and time. Notably, the HHVs of sample 260-8 and 260–12 reached 26.1 MJ·kg^{-1} and 27.2 MJ·kg^{-1}, respectively, equivalent to the heating value of high-rank coals according to the Chinese National Standard (GB/T15224.3-2004) and close to the value of hydrochar obtained by HTC of wheat straw under the same condition (Reza et al., 2015). The elevation of HHVs was significantly associated with the change of the fixed carbon and volatile matters during HTC process. And the energy yield of derived hydrochars was relatively high (60–80%), indicating that HTC is an effective way to upgrade the HHV of biomass (Yang et al., 2016).

Further insights into chemical evolution of the TSs and hydrochars were obtained with the aid of FTIR (Fig. S4, see Supplementary Information). The FTIR spectrum of the raw TSs depicted typical features of lignocellulosic biomass, similar to the published literatures (Evans, 1991; Reza et al., 2016; Sevilla et al., 2011a): the bands at 3700–3000 cm^{-1} and approximately 2900 cm^{-1} are attributed to stretching vibrations of O—H stretching and aliphatic C—H, respectively; the band around 1730 cm^{-1} corresponds to C=O of hemicellulose; 1622 cm^{-1} and 1513 cm^{-1} are assigned to aromatic ring vibrations of the lignin (the latter mainly to guaiacyl

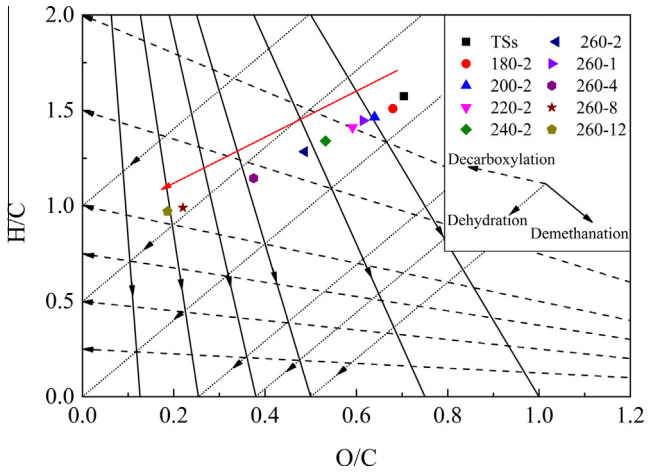

Fig. 1. Van Krevelen diagram for TSs and its hydrothermal products at different conditions.

Table 2
Elemental analysis and hydrochar yield of TSs and hydrochars.

Sample	Yield (wt.%)	Elemental analysis (wt.%)						
		N	C	H	S	O	O/C[a]	H/C[a]
TSs	–	2.37	46.22	6.06	0.57	43.38	0.70	1.57
180-2	80	2.11	46.45	5.84	0.46	42.06	0.68	1.51
200-2	67	2.06	47.22	5.77	0.45	40.28	0.64	1.47
220-2	61	2.21	48.50	5.70	0.42	38.24	0.59	1.41
240-2	63	2.34	51.98	5.81	0.41	36.91	0.53	1.34
260-2	59	2.38	52.66	5.64	0.38	34.15	0.49	1.28
260-1	62	2.16	47.39	5.72	0.31	38.84	0.61	1.45
260-4	53	3.07	55.22	5.27	0.35	27.62	0.38	1.14
260-8	43	4.24	63.03	5.20	0.37	18.51	0.22	0.99
260-12	41	4.46	65.24	5.28	0.38	16.22	0.19	0.97

[a] O/C and H/C are given in molar ratio.

Table 3
Proximate analysis, HHV and energy yield of TSs and hydrochars.

Sample	Proximate analysis (wt.%)				HHV[a] (MJ kg^{-1})	Energy yield[b] (%)
	M	VM	FC	Ash		
TSs	6.65	75.11	15.19	3.05	18.78	–
180-2	5.57	75.67	15.60	3.16	18.72	79.74
200-2	4.14	73.57	18.50	3.79	19.07	67.73
220-2	3.60	71.75	20.60	4.05	19.65	64.17
240-2	3.36	69.67	23.02	3.95	21.12	71.24
260-2	3.70	64.96	26.77	4.57	21.42	66.94
260-1	3.98	73.44	19.71	2.87	19.23	63.83
260-4	2.44	52.78	38.36	6.42	22.52	63.56
260-8	1.62	43.35	47.55	7.48	26.09	60.21
260-12	1.32	42.44	48.75	7.49	27.18	59.84

[a] HHV = 0.3491C + 1.1783H + 0.1005S − 0.1034O − 0.0151N − 0.0211Ash (MJ kg^{-1}).
[b] Hydrochar yield × $HHV_{hydrochar}/HHV_{feedstock}$.

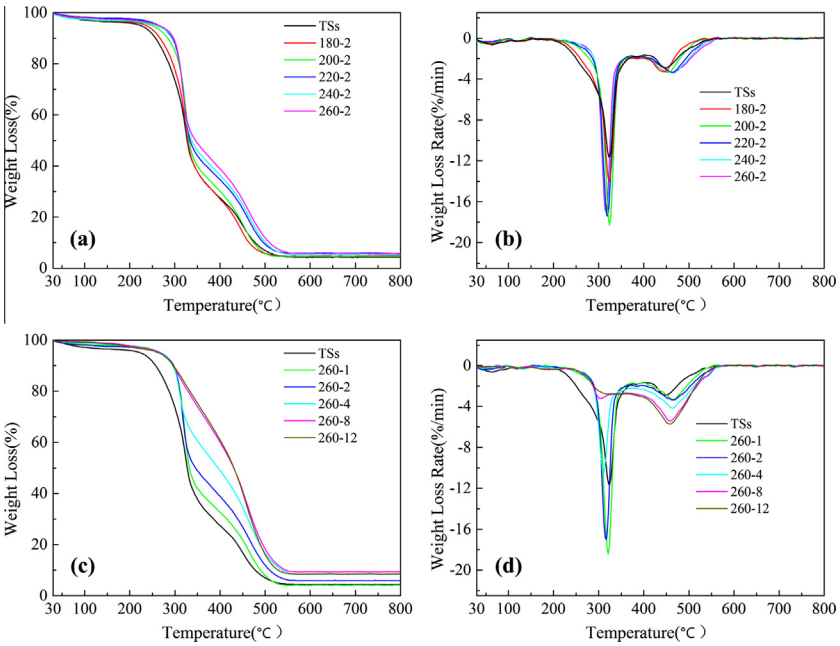

Fig. 2. TG and DTG curves of TSs and corresponding hydrochars: (a–b) different reaction temperature; (c–d) different holding time.

Table 4
Weight loss at different temperature intervals during combustion of raw TSs and hydrochar samples.

Sample	Zone 1		Zone 2		Zone 3	
	Temperature intervals (°C)	Weight loss (%)	Temperature intervals (°C)	Weight loss (%)	Temperature intervals (°C)	Weight loss (%)
TSs	30–190	3.91	190–380	65.10	380–540	26.58
180-2	30–190	3.51	190–380	65.52	380–540	26.24
200-2	30–220	3.66	220–370	60.68	370–540	30.97
220-2	30–225	2.78	225–370	57.25	370–560	33.89
240-2	30–230	3.69	230–370	54.34	370–560	36.44
260-2	30–240	3.70	240–365	50.67	365–560	39.68
260-1	30–230	2.78	230–370	59.27	370–550	33.88
260-4	30–240	3.32	240–365	39.77	365–580	48.59
260-8	30–245	3.64	245–375	29.18	375–580	57.84
260-12	30–240	3.74	240–375	27.94	375–580	59.95

units); the bands at 1457 cm^{-1} and 1423 cm^{-1} are denoted as C—H deformation in the lignin and carbohydrates, whereas 1375 cm^{-1} and 1319 cm^{-1} can be respectively attributed to C—H deformation in the cellulose/hemicellulose and the ring breathing vibrations of syringyl units in lignin; the wide band at around 1000 cm^{-1}, corresponding to C—O of alcohol, which splits into several bands at 1028 cm^{-1}, 1057 cm^{-1}, 1110 cm^{-1} and 1163 cm^{-1}, are assigned to C—O bonds of cellulose/hemicellulose and aromatic chars; and around 900 cm^{-1} is attributed to C—H deformation in the cellulose, while 780 cm^{-1} is aromatic C—H out-of-plane bending vibrations. The spectra of the raw TSs and hydrochars obtained at different temperatures with a constant holding time of 2 h exhibited several differences. There was a steady decrease on the intensity of O—H with the increase of reaction temperature, indicating that the HTC process improved the dehydration of TSs, consistent with the elemental analysis results. The bands at 1622 cm^{-1}, 1513 cm^{-1} and 1319 cm^{-1} were increasingly stronger, while the wavenumbers of 1375 cm^{-1} and 899 cm^{-1} became weaker with the increase of HTC temperature. This can be ascribed to the breakdown of cellulose/hemicellulose and partly decomposition of the stable lignin. Meanwhile, the band at 1735 cm^{-1} disappeared at a temperature higher than 200 °C, which implies the decomposition of hemicellulose structures at such temperature, similar to previous reports (Reza et al., 2013; Xiao et al., 2012). The band corresponding to aromatic carbon structures (780 cm^{-1}) was increasingly apparent after HTC treatment, demonstrating that aromatization reaction happened during such process (Sevilla and Fuertes, 2009a). It is worth noting that more significant differences can be seen in the FTIR spectra of hydrochars derived at 260 °C with different operation times. Except for the further dehydration process and aromatization reaction as well as the degradation of cellulose/hemicellulose/lignin with the extended reaction time, the lignocellulosic structures were almost completely destroyed for samples 260-8 and 260-12, since the bands corresponding to the major functional groups were disappeared, or nearly disappeared. These results are in good agreement with the elemental and proximate analysis above.

3.3. Combustion behaviors analysis

The combustion behaviors of the raw TSs and derived hydrochars were analyzed by TGA in air, the results are illustrated in Fig. 2. It could be seen that the whole combustion process of these samples depicted three distinct zones according to the DTG curves. Zone 1, 2, 3 represented the water evaporation phase, devolatilization and combustion phase, char combustion phase, respectively (Peng et al., 2016). The weight loss at different temperature intervals during combustion of raw TSs and hydrochar samples was

Table 5
Characteristic parameters of raw TSs and hydrochars during combustion.

Sample	T_0 (°C)	Peak temperature (°C)		T_f (°C)	Residues (%)
		Zone 2	Zone 3		
TSs	287.1	323.6	451.5	541.0	4.23
180-2	294.4	323.3	440.3	529.4	4.62
200-2	303.7	324.1	451.2	534.5	4.59
220-2	301.9	319.6	462.9	547.0	6.02
240-2	302.5	317.9	465.0	549.5	5.40
260-2	302.2	316.1	465.3	554.5	5.76
260-1	303.8	320.8	466.7	544.5	3.98
260-4	295.4	311.0	463.5	558.5	8.48
260-8	334.7	308.1	459.4	556.0	9.37
260-12	342.8	316.8	457.4	551.0	8.56

obtained from the analyses of TG-DTG curves and summarized in Table 4. For the TSs, the first zone was in the range of 30–190 °C and the weight loss was only 3.9%, indicating the samples contained relatively little water, the second zone with a weight loss of 65.1% was between 190 °C and 380 °C, and from 380 °C to 540 °C was the third zone which possessed a weight loss of 26.6%. The weight loss in zone 1 was rather small and barely changed with the increase of HTC reaction temperature and time from the series of combustion, which may be related to the hydrophobic property of TSs and hydrochars (He et al., 2013). Nevertheless, there was an obvious decrease of weight loss and a gradually narrowed temperature intervals in zone 2 with the increment of operation temperature and this trend became more remarkable under a longer reaction time, e.g., the weight loss decreased dramatically to 39.8–27.9% and the intervals shifted to 240–375 °C when reaction time was longer than 4 h (260-4, 260-8 and 260-12). Zone 3, in contrast, was of the opposite trend, the weight loss and temperature intervals both increased with the increase of operating temperature and time. These results could be attributed to the decomposition and carbonization process of lignocellulosic structures during HTC reaction, which resulted in increasingly lower volatile matters (devolatilization at 150–350 °C) and higher fixed carbon (combustion at 350–550 °C), consistent with the analyses in part 3.2, and therefore lead to an increasingly lower weight loss in zone 2 while the weight loss in zone 3 became increasingly higher (Peng et al., 2016; Xiao et al., 2012).

Table 5 summarizes the characteristic parameters (T_0, peak temperature, T_f and residues) obtained from the combustion of raw TSs and hydrochars. T_0 increased from 287.1 °C to around 300 °C after HTC reaction with a residence time shorter than 4 h, while it increased significantly to 334.7 °C and 342.8 °C for 260-8 and 260-12, respectively. This can be associated with the decrease of volatile matters. According to previous research, a higher T_0 may be advantageous in avoiding potential fire hazard and minimizing explosion risks when using such hydrochars as solid fuel (Xu and Sheng, 2012). The increase in T_f and the peak temperature in zone 3 after HTC treatment may be due to the increase of fixed carbon. Comparing to the raw TSs, the peak temperature of zone 2 for hydrochar samples shifted to a lower value possibly due to the destruction of long chain polymers such as hemicellulose and cellulose into short chain active small-molecule matters (Hoekman et al., 2011). The changes in residue levels were in accordance with the ash contents in proximate analysis, and the high residues of hydrochars derived under a relatively long operation time ($\geqslant$4 h) indicate that in order to obtain high quality solid fuel from HTC treated TSs the reaction time must be appropriate.

3.4. Kinetic analysis

The determination of kinetic parameters is of great significance for better understanding of combustion behaviors of the raw TSs and the derived hydrochars, both mechanistically and for potential pilot-scale expansion of the process. Activation energy and pre-exponential factor are two crucial kinetic parameters to estimate the energy barrier and intensity of combustion reactions for the fuels (He et al., 2013). According to the fitting results of linear regression using the expressions of $G(\alpha)$ for the basic model functions shown in Table S1, model F1 and D3 presented the highest correlation coefficients for the second and third combustion zone for all the samples, respectively. Table 6 is a summary of the kinetic parameters of raw TSs and hydrochars. The correlation coefficients of zone 2 were between 0.9314 and 0.9887. The hydrochars prepared at different temperature showed relatively higher activation energy than the raw TSs (46.1 kJ/mol) in zone 2 and the activation energy gradually increased with the elevation of HTC temperatures, which can be attributed to the decomposition of relative reactive compounds and the release of unstable volatile matters during HTC process (Funke and Ziegler, 2010; Yang et al., 2016). It is worth noting that the activation energy began to decrease with a reaction time longer than 2 h at a constant temperature of 260 °C, probably because the lignocellulosic structures were severely destroyed and the highly amorphous carbonaceous structure was formed under such conditions. Zone 3 was fitted by model D3 with comparatively high correlation coefficients ranging from 0.9551 to 0.9943. The activation energy of TSs in zone 3 was 41.5 kJ/mol, lower than that of hydrochar samples which ranged from 46.7 kJ/mol to 85.8 kJ/mol. Interestingly, the activation energy kept constant at around 50 kJ/mol for 200-2, 220-2, 240-2 and 260-2 samples, while it increased dramatically to 60.6 kJ/mol, 83.4 kJ/mol and 85.8 kJ/mol for 260-4, 260-8 and 260-12 samples, respectively. This may be explained by the differences of fixed carbon of the raw TSs and hydrochars shown in Table 3, since zone 3 is mainly dominated by the combustion of fixed carbon (Peng et al., 2016). According to the results aforementioned, the calculated kinetic parameters could be applied to predict the combustion behaviors

Table 6
Combustion kinetic parameters for TSs and hydrochars.

Sample	Zone 2					Zone 3				
	Temperature intervals (°C)	E (kJ/mol)	A (min^{-1})	Mechanism	R^2	Temperature intervals (°C)	E (kJ/mol)	A (min^{-1})	Mechanism	R^2
TSs	190–380	46.1	9.36E+02	F1	0.9656	380–540	41.5	2.48E+01	D3	0.9800
180-2	190–380	49.2	1.71E+03	F1	0.9453	380–540	46.7	7.54E+01	D3	0.9806
200-2	220–370	62.2	2.50E+04	F1	0.9358	370–540	50.7	1.45E+02	D3	0.9675
220-2	225–370	69.7	1.15E+05	F1	0.9330	370–560	50.2	1.08E+02	D3	0.9639
240-2	230–370	67.5	6.91E+04	F1	0.9164	370–560	50.0	9.34E+01	D3	0.9669
260-2	240–365	74.8	3.23E+05	F1	0.9286	365–560	50.4	7.54E+01	D3	0.9698
260-1	230–370	74.7	3.32E+05	F1	0.9423	370–550	47.9	6.97E+01	D3	0.9551
260-4	240–365	66.3	4.36E+04	F1	0.9467	365–580	60.6	4.56E+02	D3	0.9830
260-8	245–375	48.1	5.46E+02	F1	0.9846	375–580	83.4	1.98E+04	D3	0.9943
260-12	240–375	43.7	1.93E+02	F1	0.9876	375–580	85.8	3.01E+04	D3	0.9892

of TSs and derived hydrochars during combustion, for examples, in a fixed or fluidized bed boiler type of applications.

4. Conclusion

The morphologies of raw TSs were destroyed after HTC. The carbon contents of hydrochars increased to 46.5–65.2%, while hydrogen and oxygen contents decreased to 5.2–5.8% and 16.2–42.1%, respectively. The obtained hydrochars possessed lower volatile (42.4–75.7%), higher fixed carbon (15.6–48.8%) and higher HHV (18.7–27.2 MJ kg^{-1}). The TSs and hydrochars both exhibited small BET surface areas and poor porosity. The weight loss, combustion temperature intervals and characteristic temperatures of the raw TSs and hydrochars during combustion were different. The activation energy of hydrochars in zone 2 and 3 were among 43.7–74.8 kJ/mol and 46.7–85.8 kJ/mol, respectively, while for TSs were 46.1 kJ/mol and 41.5 kJ/mol.

Acknowledgements

This work was supported by CNTC's projects. The authors wish to thank Dr Chuan Liu of R&D Centre of British American Tobacco for useful discussions during the preparation of this manuscript.

Appendix A. Supplementary data

Supplementary data associated with this article can be found, in the online version, at http://dx.doi.org/10.1016/j.biortech.2016.08.098.

References

Bassilakis, R., Carangelo, R.M., Wojtowicz, M.A., 2001. TG-FTIR analysis of biomass pyrolysis. Fuel 80, 1765–1786.
Coats, A.W., Redfern, J.P., 1964. Kinetic parameters from thermogravimetric data. Nature 201, 68–69.
Dudder, H., Wutscher, A., Stoll, R., Muhler, M., 2016. Synthesis and characterization of lignite-like fuels obtained by hydrothermal carbonization of cellulose. Fuel 171, 54–58.
Evans, P.A., 1991. Differentiating "hard" from "soft" woods using Fourier transform infrared and Fourier transform spectroscopy. Spectrochim. Acta Part A 47, 1441–1447.
Funke, A., Ziegler, F., 2010. Hydrothermal carbonization of biomass: a summary and discussion of chemical mechanisms for process engineering. Biofuels Bioprod. Biorefin. 4, 160–177.
Gil, M.V., Casal, D., Pevida, C., Pis, J.J., Rubiera, F., 2010. Thermal behaviour and kinetics of coal/biomass blends during co-combustion. Bioresour. Technol. 101, 5601–5608.
He, C., Giannis, A., Wang, J., 2013. Conversion of sewage sludge to clean solid fuel using hydrothermal carbonization: hydrochar fuel characteristics and combustion behavior. Appl. Energy 111, 257–266.
Hoekman, S.K., Broch, A., Robbins, C., 2011. Hydrothermal carbonization (HTC) of lignocellulosic biomass. Energy Fuels 25, 1802–1810.
Hu, R., Wang, J., Li, H., Ni, H., Chen, Y., Zhang, Y., Xiang, S., Li, H., 2015. Simultaneous extraction of nicotine and solanesol from waste tobacco materials by the column chromatographic extraction method and their separation and purification. Sep. Purif. Technol. 146, 1–7.
Huff, M.D., Kumar, S., Lee, J.W., 2014. Comparative analysis of pinewood, peanut shell, and bamboo biomass derived biochars produced via hydrothermal conversion and pyrolysis. J. Environ. Manage. 146, 303–308.
Islam, M.A., Auta, M., Kabir, G., Hameed, B.H., 2016. A thermogravimetric analysis of the combustion kinetics of karanja (*Pongamia pinnata*) fruit hulls char. Bioresour. Technol. 200, 335–341.
Islam, M.A., Kabir, G., Asif, M., Hameed, B.H., 2015. Combustion kinetics of hydrochar produced from hydrothermal carbonisation of Karanj (*Pongamia pinnata*) fruit hulls via thermogravimetric analysis. Bioresour. Technol. 194, 14–20.
Kambo, H.S., Dutta, A., 2015. Comparative evaluation of torrefaction and hydrothermal carbonization of lignocellulosic biomass for the production of solid biofuel. Energy Convers. Manage. 105, 746–755.
Kang, S., Li, X., Fan, J., Chang, J., 2012. Characterization of hydrochars produced by hydrothermal carbonization of lignin, cellulose, D-xylose, and wood meal. Ind. Eng. Chem. Res. 51, 9023–9031.
Kilic, M., Apaydin-Varol, E., Putun, A.E., 2011. Adsorptive removal of phenol from aqueous solutions on activated carbon prepared from tobacco residues: equilibrium, kinetics and thermodynamics. J. Hazard. Mater. 189, 397–403.
Lai, Z., Ma, X., Tang, Y., Lin, H., Chen, Y., 2012. Thermogravimetric analyses of combustion of lignocellulosic materials in N_2/O_2 and CO_2/O_2 atmospheres. Bioresour. Technol. 107, 444–450.
Li, W., Zhang, L., Peng, J., Li, N., Zhu, X., 2008. Preparation of high surface area activated carbons from tobacco stems with K_2CO_3 activation using microwave radiation. Ind. Crops Prod. 27, 341–347.
Li, X., Lv, Y., Ma, B., Jian, S., Tan, H., 2011. Thermogravimetric investigation on co-combustion characteristics of tobacco residue and high-ash anthracite coal. Bioresour. Technol. 102, 9783–9787.
Liu, Z., Balasubramanian, R., 2012. Hydrothermal carbonization of waste biomass for energy generation. Proc. Environ. Sci. 16, 159–166.
Parshetti, G.K., Kent Hoekman, S., Balasubramanian, R., 2013. Chemical, structural and combustion characteristics of carbonaceous products obtained by hydrothermal carbonization of palm empty fruit bunches. Bioresour. Technol. 135, 683–689.
Peng, C., Zhai, Y., Zhu, Y., Xu, B., Wang, T., Li, C., Zeng, G., 2016. Production of char from sewage sludge employing hydrothermal carbonization: char properties, combustion behavior and thermal characteristics. Fuel 176, 110–118.
Ragauskas, A.J., Williams, C.K., Davison, B.H., Britovsek, G., Cairney, J., Eckert, C.A., Frederick, W.J., Hallett, J.P., Leak, D.J., Liotta, C.L., Mielenz, J.R., Murphy, R., Templer, R., Tschaplinski, T., 2006. The path forward for biofuels and biomaterials. Science 311, 484–489.
Reza, M.T., Lynam, J.G., Uddin, M.H., Coronella, C.J., 2013. Hydrothermal carbonization: fate of inorganics. Biomass Bioenergy 49, 86–94.
Reza, M.T., Rottler, E., Herklotz, L., Wirth, B., 2015. Hydrothermal carbonization (HTC) of wheat straw: influence of feedwater pH prepared by acetic acid and potassium hydroxide. Bioresour. Technol. 182, 336–344.
Reza, M.T., Yang, X., Coronella, C.J., Lin, H., Hathwaik, U., Shintani, D., Neupane, B.P., Miller, G.C., 2016. Hydrothermal carbonization (HTC) and pelletization of two arid land plants bagasse for energy densification. ACS Sustainable Chem. Eng. 4, 1106–1114.
Sevilla, M., Antonio Macia-Agullo, J., Fuertes, A.B., 2011a. Hydrothermal carbonization of biomass as a route for the sequestration of CO_2: chemical and structural properties of the carbonized products. Biomass Bioenergy 35, 3152–3159.
Sevilla, M., Fuertes, A.B., 2009a. Chemical and structural properties of carbonaceous products obtained by hydrothermal carbonization of saccharides. Chem. Eur. J. 15, 4195–4203.
Sevilla, M., Fuertes, A.B., 2009b. The production of carbon materials by hydrothermal carbonization of cellulose. Carbon 47, 2281–2289.
Sevilla, M., Fuertes, A.B., Mokaya, R., 2011b. High density hydrogen storage in superactivated carbons from hydrothermally carbonized renewable organic materials. Energy Environ. Sci. 4, 1400–1410.
Sha, Y., Lou, J., Bai, S., Wu, D., Liu, B., Ling, Y., 2015. Facile preparation of nitrogen-doped porous carbon from waste tobacco by a simple pre-treatment process and their application in electrochemical capacitor and CO_2 capture. Mater. Res. Bull. 64, 327–332.
Song, G., Xiao, J., Zhao, H., Shen, L., 2012. A unified correlation for estimating specific chemical exergy of solid and liquid fuels. Energy 40, 164–173.
Titirici, M.-M., Antonietti, M., Baccile, N., 2008. Hydrothermal carbon from biomass: a comparison of the local structure from poly-to monosaccharides and pentoses/hexoses. Green Chem. 10, 1204–1212.
Van, K.D., 1950. Graphical statistical method for the study of structure and reaction processes of coal. Fuel 29, 269–284.
White, J.E., Catallo, W.J., Legendre, B.L., 2011. Biomass pyrolysis kinetics: a comparative critical review with relevant agricultural residue case studies. J. Anal. Appl. Pyrol. 91, 1–33.
Xiao, L., Shi, Z., Xu, F., Sun, R., 2012. Hydrothermal carbonization of lignocellulosic biomass. Bioresour. Technol. 118, 619–623.
Xu, M., Sheng, C., 2012. Influences of the heat-treatment temperature and inorganic matter on combustion characteristics of cornstalk biochars. Energy Fuels 26, 209–218.
Yang, W., Wang, H., Zhang, M., Zhu, J., Zhou, J., Wu, S., 2016. Fuel properties and combustion kinetics of hydrochar prepared by hydrothermal carbonization of bamboo. Bioresour. Technol. 205, 199–204.
Yang, Z., Zhang, S., Liu, L., Li, X., Chen, H., Yang, H., Wang, X., 2012. Combustion behaviours of tobacco stem in a thermogravimetric analyser and a pilot-scale fluidized bed reactor. Bioresour. Technol. 110, 595–602.
Zhao, P., Shen, Y., Ge, S., Chen, Z., Yoshikawa, K., 2014. Clean solid biofuel production from high moisture content waste biomass employing hydrothermal treatment. Appl. Energy 131, 345–367.
Zhao, Y., Lu, M., Tao, P., Zhang, Y., Gong, X., Yang, Z., Zhang, G., Li, H., 2016. Hierarchically porous and heteroatom doped carbon derived from tobacco rods for supercapacitors. J. Power Sources 307, 391–400.